

Stability-ensured topology optimization of boom structures with volume and stress considerations

Wenjun Li^{1,2} · Qicai Zhou¹ · Zhen Jiang² · Jiadong Deng² · Wei Chen²

Received: 14 August 2014 / Revised: 30 April 2016 / Accepted: 2 June 2016 / Published online: 17 June 2016
© Springer-Verlag Berlin Heidelberg 2016

Abstract The boom structure is a key component of giant boom cranes, and the stability-ensured topology optimization is critical to its lightweight design. The finite difference method, direct differentiation or adjoint method needs many time-consuming nonlinear analyses for this problem with a large number of design variables and constraints, and the last two methods are difficult to implement in off-the-shelf softwares. To overcome these challenges, this work first defines a global stability index to measure the global stability of the whole structure, and a compression member stability index to identify the buckling of compression members. Numerical and experimental verifications of these two stability indices are conducted by analyzing a simple three-dimensional frame. Next, the anti-buckling mechanism of boom structures is analyzed to develop the precedence order of freezing relative web members. The stability indices and the freezing measure are then utilized as a part of a novel Stability-Ensured Soft Kill Option (SSKO) algorithm, built upon the existing Soft Kill

Option (SKO) method. The objective is to minimize the discrepancy between structural volume and predetermined target volume, while the global stability and stress are regarded as constraints. Lastly, the SSKO algorithm with different scenarios is applied to topology optimization problems of four-section frames and a ring crane boom; in both cases the consistent and stable topologies exhibit applicability of the proposed algorithm.

Keywords Boom structures · Topology optimization · Stability index · Stability-ensured soft kill option · Geometric nonlinearity

1 Introduction

The use of giant boom cranes has gained an ever-increasing popularity due to their superior handling abilities. As boom structures are equipped on boom cranes for hoisting cargos, lightweight design of a giant boom structure, which is usually achieved by topology optimization, becomes critical in reducing the energy consumption of the whole crane and hence draws much research attention recently. In topology optimization of giant boom structures, geometrically nonlinear analysis has been adopted to capture the accurate structural response. A common issue is that the stiffness of some members keeps decreasing during the optimization process, which is often a generator of some slender struts leading to buckling issues. Therefore, a stability-ensured topology optimization algorithm for structural design is needed to maintain sufficient stability of boom structures while reducing the weight and manufacturing costs.

The stability performance is studied either as a constraint or as an objective in topology optimization problems (Ohsaki and Ikeda 2007). The most popular algorithms for topology

✉ Wei Chen
weichen@northwestern.edu

Wenjun Li
wenjun.li.nu@gmail.com

Qicai Zhou
qczhou@tongji.edu.cn

Zhen Jiang
ZhenJiang2015@u.northwestern.edu

Jiadong Deng
jiadongdeng2012@u.northwestern.edu

¹ School of Mechanical Engineering, Tongji University, Shanghai, Shanghai 201804, China

² Department of Mechanical Engineering, Northwestern University, Evanston, IL 60208-3111, USA

optimization with stability considerations are gradient-based methods utilizing sensitivity analysis of buckling load factors. The evolutionary structural optimization (ESO) method was extended to buckling problems, and a simple method not involving variational calculus or Lagrangian multipliers was presented for the optimum design of columns and frames to enhance the elastic buckling resistance of structures (Manickarajah et al. 2000). Kemmler et al. (Kemmler et al. 2005) considered the lowest critical load level as an inequality constraint and conducted topology optimization of structures including kinematics based on the sensitivities of the design criteria. The design problem of maximizing the buckling load factor of laminated multi-material composite shell structures was investigated using the discrete material optimization approach, which solves discrete optimization problems using gradient-based techniques and mathematical programming (Lindgaard and Lund 2010, 2011; Lund 2009). Lindgaard and Dahl (Lindgaard and Dahl 2013) investigated a range of different compliance and buckling objective functions for maximizing the buckling resistance of a snap-through beam structure.

The gradient-based optimization methods have been widely used in topology optimization problems with a couple of stability constraints, since sensitivities can be obtained efficiently using the finite difference method, adjoint method or direct differentiation (Tortorelli and Michaleris 1994). A fundamental premise of optimizing large-scale boom structures is to capture their nonlinear behaviors accurately. Since the computational accuracy usually can be ensured by an off-the-shelf finite element analysis (FEA) software, resorting to a commercial software is an appropriate way to realize our own optimization algorithms for large-scale structures. However, for a problem with 1000 variables and 1000 constraints, 1000 evaluations will be required for the sensitivity analysis if the finite difference method, direct differentiation or adjoint method is applied, which are still extremely expensive due to 1000 times of time-consuming nonlinear analyses. In addition, for commercial softwares, the integration of adjoint method or direct differentiation method for sensitivity analysis is not an easy task, as the adjoint field with appropriate load and displacement boundary conditions needs to be defined and solved (tangent operator involved for geometrically nonlinear problems). Hence, these three methods are not applicable due to huge computational cost and the adjoint method or direct differentiation is difficult to implement in commercial softwares. Furthermore, the large number of constraints can be collected in a single constraint by smooth envelope functions or constraint aggregations like the p -norm or *Kreisselmeier-Steinhauser* (K-S) functions (Duysinx and Sigmund 1998; Rozvany and Sobieszczanski-Sobieski 1992; Sigmund and Maute 2013), but for nonlinear bars structures, it becomes rather complicated to compute buckling constraints for the aggregation function, since the nonlinear stability levels and

buckling load factors are captured based on the equilibrium path of each member. Besides, there are different aggregate functions, and each aggregate function has different penalty parameters. Whether these aggregate functions can be successfully integrated into this highly nonlinear buckling problem is still unknown. Hence, we do not apply these constraint aggregation techniques for our research problem. Lastly, only a few efforts on reducing the computational cost associated with topology optimization involving buckling can be found in existing literature. Browne et al. (Browne et al. 2012) proposed a fast binary descent method to reduce the number of derivative calculations required in topology optimization of linear elastic structures subject to compliance and buckling constraints. Hjelmstad and Pezeshk (Hjelmstad and Pezeshk 1991) presented an optimization-based design procedure capable of improving the limit behavior of space frames without resorting to nonlinear analyses, which enhances the inelastic stability of a structure by maximizing its linearized buckling eigenvalues.

In the presence of aforementioned inconvenience of pure gradient-based methods, zero-order or hybrid methods are put forward to provide a convenient way for topology optimization of geometrically nonlinear boom structures. The Soft Kill Option (SKO) method is a fully stressed topology optimization method like the Evolutionary Structural Optimization (ESO) method (Baumgartner et al. 1992; Eschenauer and Olhoff 2001), and the fully stressed method usually converges in dozens of iterations and does not depend on structure size (Cheng 2012), so the SKO method is particularly applicable for large-scale structures. Even though sensitivity analysis is not used, the topology results obtained with the SKO method are very similar to those by gradient-based methods using OptiStruct (Harzheim and Graf 2005, 2006). Our previous work (Li et al. 2013) has extended the SKO method into topology optimization of linear bars structures which sets the foundation for this research.

Both global stability and member stability need quantitative evaluation in the optimization process while the strength status is indicated through a variety of stresses, e.g., von Mises stress. A couple of member buckling judgment methods for bars structures have been presented in recent years. Shen et al. (Shen et al. 2007) proposed a middle plastic hinge model of the member, assuming that the member is in a completely elastic deformation condition before buckling, and that a plastic hinge would appear in the middle of the member when the internal force exceeds the bearing capacity of the member. Fan et al. (Fan et al. 2012) adopted the curve of axial force-relative deflection of the member and the energy method to judge the member buckling of reticulated shell structures; however the energy method is only adequate for elastic structures. To better monitor the stability of the structure, global stability index (GSI) and compression member stability index (MSI) are defined in this paper. The global stability status can be easily

formulated by GSI, while member buckling of any compression member can be detected by MSI. The imperfection and pre-buckling deformation always exist in actual engineering structures, therefore limit-point, flexural or flexural-torsional buckling of compression members are common; by contrast bifurcation and torsional buckling rarely occur (Chen 2011). The presented MSI is capable of detecting the limit-point, elastic or elastoplastic, flexural or flexural-torsional buckling of compression members only considering the end forces, which will be verified by numerical analysis and physical experiment later in this paper.

Apart from stability, the volume and stress should also be taken into consideration in topology optimization of boom structures so that the topology design is close to industrial application. However, it is very difficult to find optimization algorithms for discrete problems that can treat multiple non-trivial constraints (Sigmund and Maute 2013). So far, only a few papers have addressed the discrete topology optimization problems with multiple (non-volume) constraints (Bojczuk and Mroz 1999; Pyrz 1990). The traditional volume constraint always conflicts with global stability and stress constraints, thus the predetermined target volume fraction may not be achieved. Adaptive volume constraint algorithm is proposed in Lin and Sheu (Lin and Sheu 2009) so that the maximum stress in the optimal structural configuration is guaranteed to be below the predefined stress limit. In this work, the traditional volume constraint is replaced by an objective function of minimizing the discrepancy between structural volume and predetermined target volume.

This paper proposes a Stability-Ensured Soft Kill Option (SSKO) algorithm for topology optimization of boom structures that reduces the amount of material and makes them close to the target volume fraction while simultaneously accounting for the predetermined maximum stress limit. In Section 2, GSI is stated to quantitatively express the global stability constraint, while MSI is defined based on the axial stiffness of a compression member. Subsequently we conduct numerical and experimental verifications of these two stability indices. Besides, the anti-buckling mechanism of boom structures is explained. In Section 3, the stability-ensured topology optimization with volume and stress considerations is formulated, and the proposed SSKO algorithm is described in detail. Section 4 presents two illustrative examples by using different optimization scenarios. Conclusions are outlined in Section 5.

2 Stability indices and anti-buckling mechanism

The concepts and physical meanings of two stability indices, the GSI and MSI, are presented hereafter. Numerical and experimental verifications of these two stability indices are conducted by analyzing a simple three-dimensional frame employing a dually (geometrically and materially)

nonlinear elastic static model. Although the stability indices are applied for boom structures in this paper, they can also be used in other kinds of bars structures. In addition, the anti-buckling mechanism of boom structures is analyzed based on the knowledge of bracing systems, and an accompanying technique of “freeze” is proposed for stability enhancement.

2.1 Global stability index

The overall stiffness of a structure reflects its global stability status, and the change of overall stiffness can be used as a judgment basis of global buckling. For a static structure, the overall stiffness can be defined as the slope of load–displacement curve of a certain position at the last convergence incremental step, represented by S_g , which can be approximated by calculating difference quotient easily. A positive S_g infers a stable structure, while zero or a negative number value means the structure is global buckling. In the process of topology optimization, we need to quantitatively express the global stability status for monitoring the global stability constraint, and the global stability index (GSI) is defined as

$$GSI^{(k)} = S_g^{(k)} / S_g^{(0)}, \quad k = 0, 1, \dots, k_{\max} \quad (1)$$

where k is the indicator of iteration number, $k=0$ means the initial analysis of the structure, and k_{\max} is the maximum number of iterations. $GSI^{(k)}$ is the global stability index in k -th iteration, and $S_g^{(k)}$ denotes the overall stiffness of the structure in k -th iteration. $GSI^{(0)}$ is equal to 1 if the whole structure is stable in the initial analysis.

The GSI is generally less than 1 in the optimization process due to the decline of the overall stiffness. Similar to the overall stiffness, a positive GSI infers a stable structure, while it decreases to zero or a negative number when the structure becomes global buckling. The GSI expresses the relative stability compared to the initial structure, which can be easily figured out upon the results of geometrically nonlinear analysis in common FEA software tools and can be applied in all kinds of static structures.

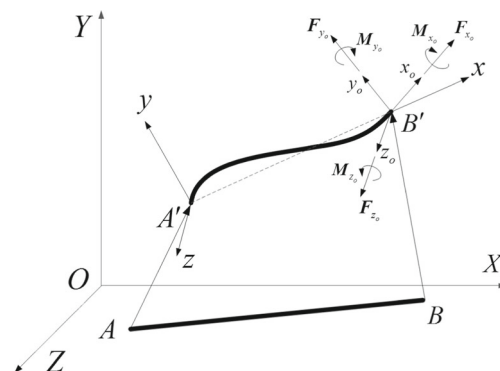


Fig. 1 Deformation of a compression member



Fig. 2 The frame model

2.2 Compression member stability index

Figure 1 shows the deformation of a compression member in the global coordinate system $O-XYZ$. AB is the initial configuration before deformation and $A'B'$ is the configuration after deformation. All non-end loads have been converted to end loads, such as gravity load and wind load. Based on the Eulerian description, the current configuration is taken as the reference configuration then the end loads and end displacements of a compression member can be easily formulated (Mase and Mase 1999). Therefore, two local coordinate systems, the member coordinate system $A'-xyz$ and the member end coordinate system $B'-x_0y_0z_0$, are defined as follows. In the member coordinate system: the direction of vector $\overrightarrow{A'B'}$ (pointing from A' to B') is defined as $+x$ direction, $+y$ direction is parallel to plane XY and its angle with $+Y$ is smaller than or equal to 90° ; in the case when axial x is parallel to axial Z , axial y is defined to be parallel to axial Y . In the member end coordinate system, the outward tangential direction at B' is defined as $+x_0$ direction, $+y_0$ direction is parallel to plane XY and its angle with $+Y$ is smaller than or equal to 90° ; similarly to the member coordinate system, when axial x_0 is parallel to axial Z , axial y_0 is defined to be parallel to axial Y . Both local coordinate systems are right-handed and depend on the configuration after deformation. The loading condition at the

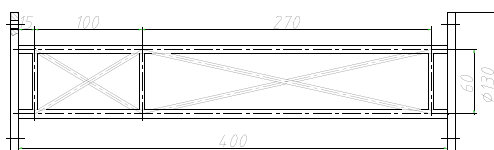


Fig. 3 Dimensions of the frame

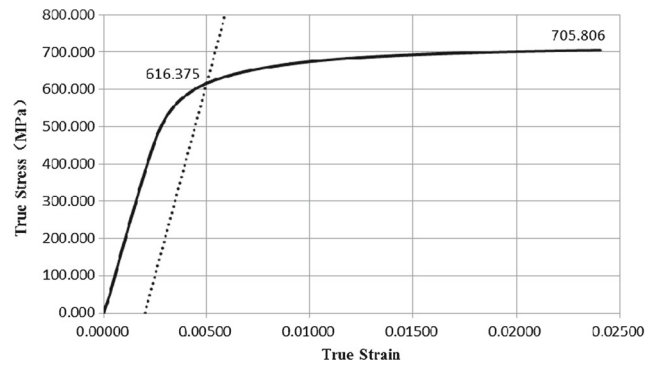


Fig. 4 True stress-ture strain curve of cold drawn round steel

end B' is expressed in the member end coordinate system (Fig. 1). They are three force components $F_{x_0}, F_{y_0}, F_{z_0}$ and three bending moments $M_{x_0}, M_{y_0}, M_{z_0}$.

The axial vector of member AB after deformation is

$$\mathbf{a} = \overrightarrow{A'B'} \tag{2}$$

The three force components $F_{x_0}, F_{y_0}, F_{z_0}$ are projected onto the axial vector, and the projection sum is the axial force of member AB after deformation

$$F_a = (\mathbf{F}_{x_0} + \mathbf{F}_{y_0} + \mathbf{F}_{z_0}) \cdot \mathbf{a} / \|\mathbf{a}\| \tag{3}$$

where $\|\cdot\|$ denotes the module of a vector, similarly hereinafter; a positive value of F_a means tension while a negative value means compression.

The axial relative displacement between the ends of member AB is written as

$$\Delta u = \|\mathbf{a}\| - \|\overrightarrow{AB}\| \tag{4}$$

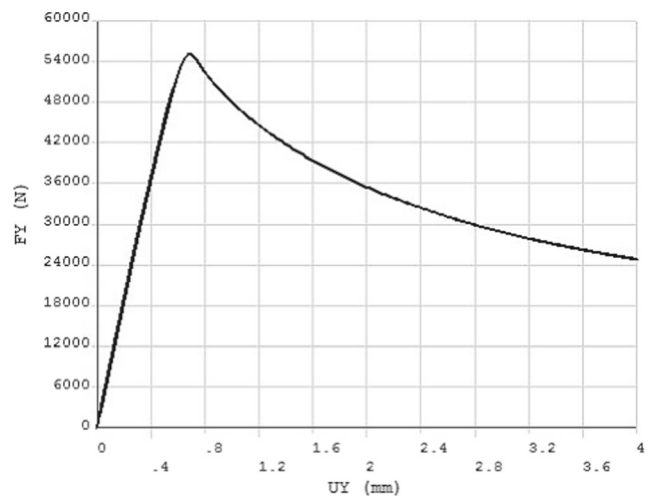


Fig. 5 Load-deflection curve of the frame

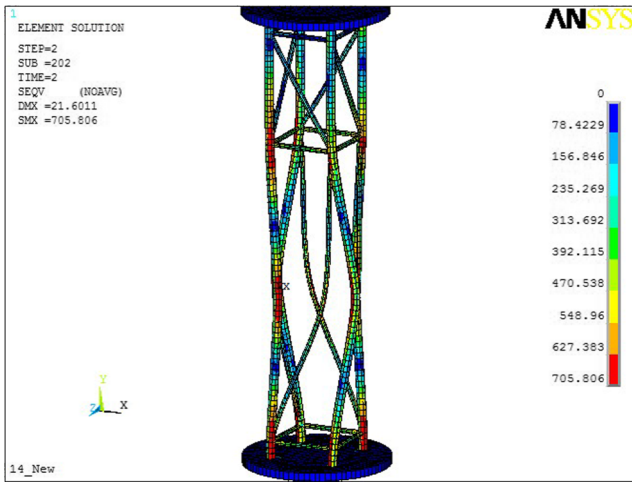


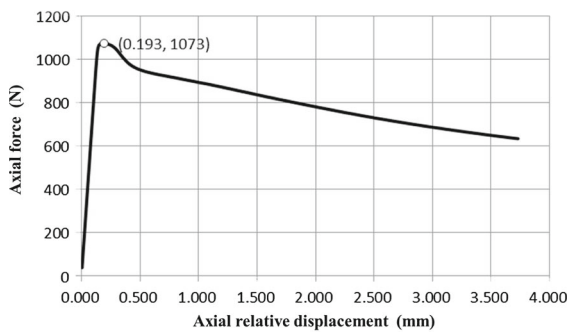
Fig. 6 Post-buckling stress contour of the frame

A positive value of Δu means elongation while a negative value means shortening.

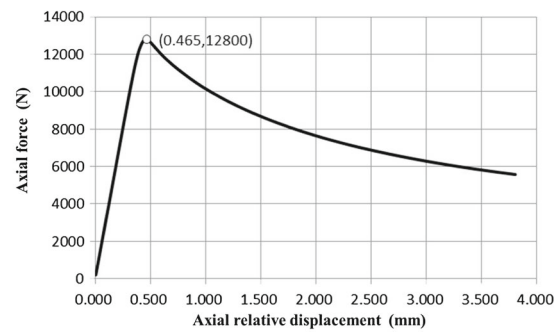
For any member AB in a frame structure, its axial stiffness at time t can be approximated by calculating difference quotient like the overall stiffness.

$${}^tS_a = ({}^tF_a - {}^{t-\Delta t}F_a) / ({}^t\Delta u - {}^{t-\Delta t}\Delta u) \quad (5)$$

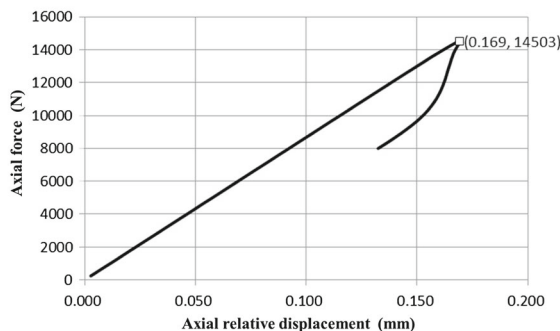
Here $t - \Delta t$ is the time with a tiny time period Δt difference prior to time t .



(a) The lower diagonal web member



(b) The lower chord member



(c) The upper chord member

Fig. 7 Axial force-axial relative displacement curves of compression members

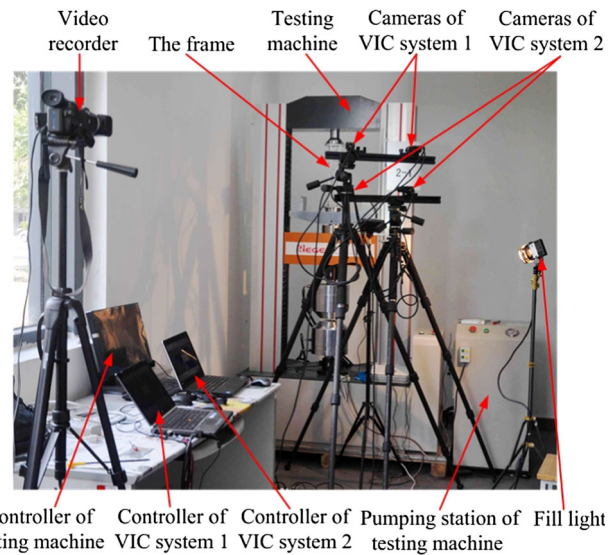


Fig. 8 Experiment scene

In engineering structures, the buckling of a compression member is identified as that when the axial compression force begins to decline and the absolute value of the axial relative displacement is still increasing. In other words, a compression member is buckling when its tS_a value changes from a positive number to a negative number. Hence, capturing the changes of axial stiffness can help judge whether a compression member is unstable.

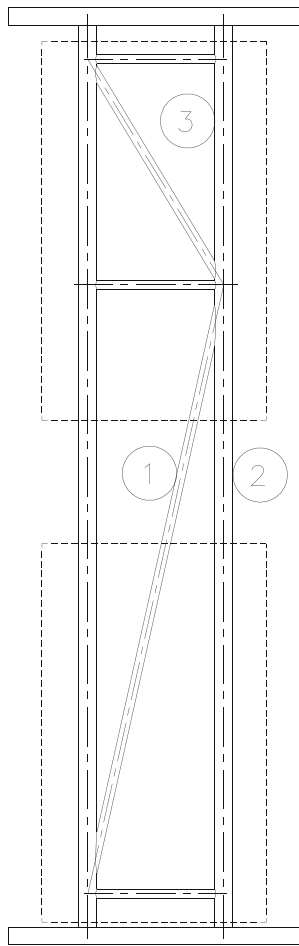


Fig. 9 Observation areas of two Vic-3D systems

In the optimization process, we can quantitatively evaluate the compression member stability status by the MSI defined as

$$MSI_{(j)}^{(k)} = S_{a(j)}^{(k)} / S_{a(j)}^{(0)}, \quad k = 0, 1, \dots, k_{\max} \quad (6)$$

where $MSI_{(j)}^{(k)}$ is the stability index of member j in the k -th iteration. $S_{a(j)}^{(k)}$ denotes the axial stiffness of member j in the k -th iteration, which is determined in Equation (5). $MSI_{(j)}^{(0)}$ is equal to 1 if member j is stable in the initial analysis. When $MSI_{(j)}^{(k)}$ decreases to zero or a negative value, the compression member j buckles.

2.3 Numerical and experimental verifications of the stability indices

A simple three-dimensional frame structure (Fig. 2) is constructed and analyzed to verify the proposed stability indices. This frame is welded by cold drawn round steel and hot rolled plate steel. Figure 3 gives the overall dimensions of the frame in millimeters wherein the cross sections of chord members and web members are $\phi 8(\text{mm})$ and $\phi 4(\text{mm})$ respectively. The two 8 mm-thick steel plates are used to fix chord members and

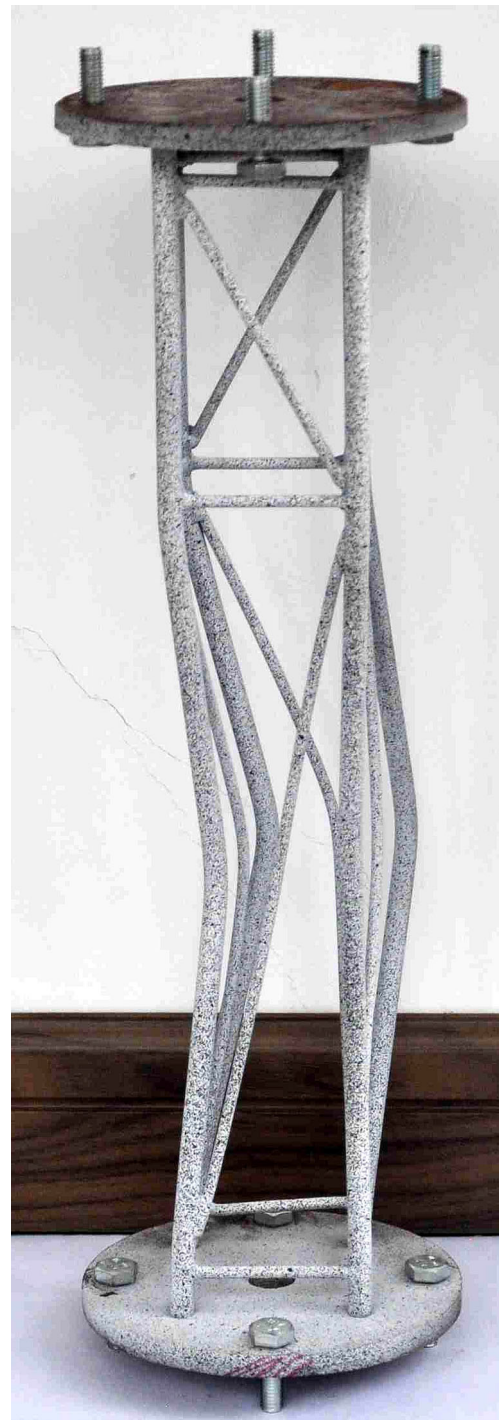


Fig. 10 The frame after unloading

transfer external loads. As shown in Fig. 2, the upper surface of the top plate is fixed and a uniform pressure along +Y direction is applied to the lower surface of the bottom plate in tests. The engineering stress–strain curve of cold drawn round steel has been experimentally determined and the true stress–strain curve is shown in Fig. 4. The elastic limit is 483 MPa, the yield strength is 616 MPa, and the ultimate strength is 705 MPa with Young's modulus being 206,000 MPa.

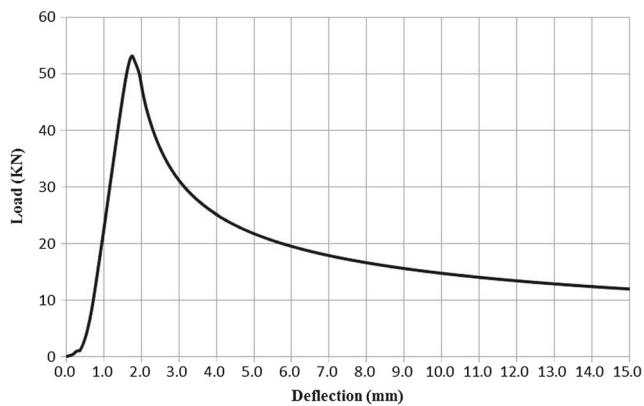


Fig. 11 Load-deflection curve in the experiment

2.3.1 Numerical analysis

We apply the Multi-linear Kinematic Hardening model to simulate the material property of the cold drawn round steel by importing the true stress-true strain data into the FE package ANSYS 13.0 (Lawrence 2011). The plates in this frame are regarded as rigid bodies for simplification. Geometrically and materially nonlinear buckling analysis of the frame is carried out based on the incremental displacement method integrated with the Newton–Raphson method (Li et al. 2015), and the obtained load-deflection curve is shown in Fig. 5. The frame archives the limit-point buckling when the load reaches 55055N, meanwhile the vertical displacement of the load-end (the lower surface of the bottom plate) comes to 0.695 mm. Figure 6 indicates the post-buckling von Mises stress distribution when +Y displacement of the load-end is 4 mm. It also shows the lower chord members and the lower diagonal web members bend significantly along with torsional deformation.

The predefined GSI, only depending on the overall stiffness of the structure, is used to distinguish global buckling of any static structure in a structural optimization process, so the correctness of GSI can be demonstrated by investigating the effectiveness of the overall stiffness. In addition, it should be noted that the overall stiffness can be figured out at any loading time as long as we define the time as the last convergence incremental step. As shown in Fig. 5, the slope of load-deflection curve changes from positive to negative which means that the overall stiffness of this frame reduces from positive to negative. The overall stiffness equals zero at the limit point of load-deflection curve and thus it can be used to detect global buckling effectively. Hence, the GSI is an accurate global buckling indicator during the optimization phase.

Similarly, analyzing the validity of the axial stiffness will certify the accuracy of MSI as the member buckling indicator. Considering a peripheral symmetric configuration of the frame, we take any set of lower diagonal web member, lower chord member and upper chord member as the observed. The axial forces and axial relative displacements are calculated upon Equations (3) and (4), and their relation curves are shown in Fig. 7. The slope of one curve is the axial stiffness

of corresponding member according to Equation (5). It should be noted that the sign of the values shown in Fig. 7 has been reversed for ease of viewing, similarly hereinafter.

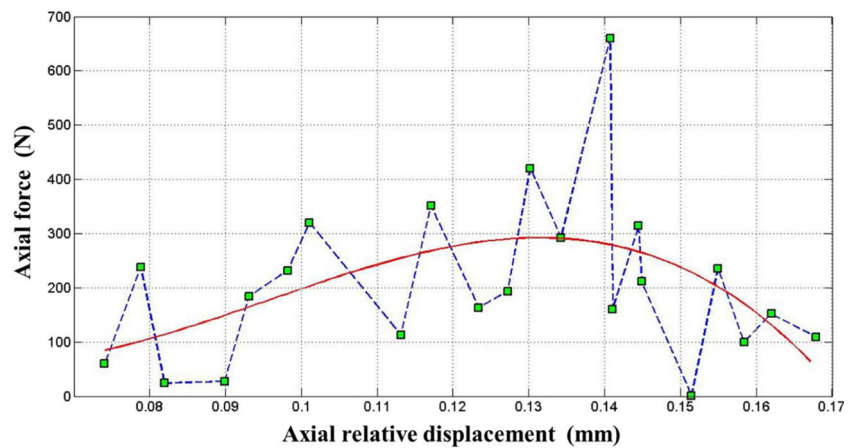
At time step 21, the lower diagonal web member loses stability since its axial stiffness becomes negative, meanwhile the axial relative displacement is -0.193 mm and the axial force is -1073 N (Fig. 7a). The maximum stress of the lower diagonal web member is 292 MPa which means elastic buckling occurs in the lower diagonal web member. At time step 36, the axial stiffness of the lower chord member decreases to a negative number and its axial relative displacement and axial force are -0.465 mm and -12800 N, respectively (Fig. 7b). The elastoplastic buckling happens in the lower chord member with the maximum stress 554 MPa and the global buckling of the frame happens at the same time. Subsequently, at time step 37, the absolute values of axial relative displacement and axial force begin to decrease while the axial stiffness remains positive, therefore springback occurs in the upper chord member and yet member buckling does not happen (Fig. 7c).

2.3.2 Experimental analysis

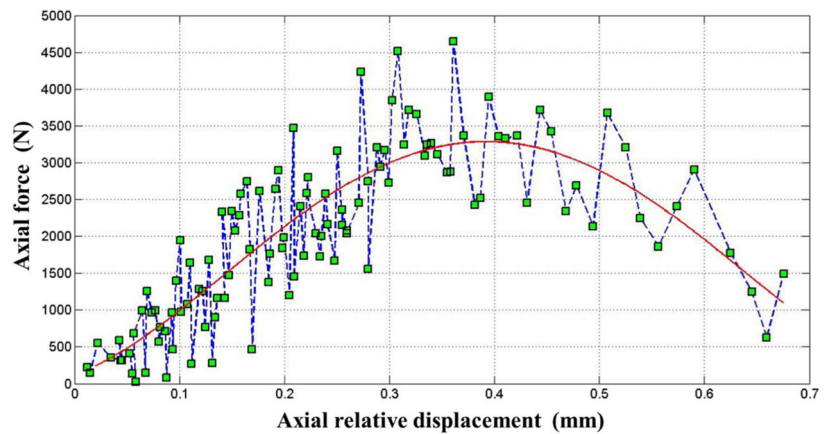
The experiment scene is depicted in Fig. 8. We mainly use a 300 kN electronic universal testing machine RGM-4300 (The electronic universal testing machine RGM-4300 2014), two non-contacting measurement systems VIC-3D (The VIC-3D System 2014) and a fill light in the buckling experiment. The 400 mm-height frame structure exceeds the measuring capacity of one VIC system, so we use two VIC systems to measure both displacement and strain of the surfaces of three compression members, as shown in Fig. 9. VIC system 1 and VIC system 2 capture data in the upper rectangular observation area and the lower rectangular observation area, respectively. The loading speed of the testing machine is set to be 0.6mm/min and its sampling frequency is 25 Hz. Besides, the maximum loading displacement is set to be 15 mm and the sampling frequency of two VIC systems is 1 Hz.

The frame after unloading is shown in Fig. 10. The lower chord members and lower diagonal web members bend dramatically with slight torsional deformation, and the upper chord members almost revert to original straight shape. The load-deflection curve of the frame recorded by the testing machine is given in Fig. 11. When the vertical displacement of the load-end reaches 1.752 mm, global buckling happens and the critical load equals 53157 N. The relative error in simulating the buckling loads compared with the experiment is -3.45% , so the accuracy of the numerical simulation is proved. In addition, experimental deflection at the buckling point is 1.752 mm, about 1 mm larger than numerical result, due to the assembling gap, imperfections and deformation of weld joints.

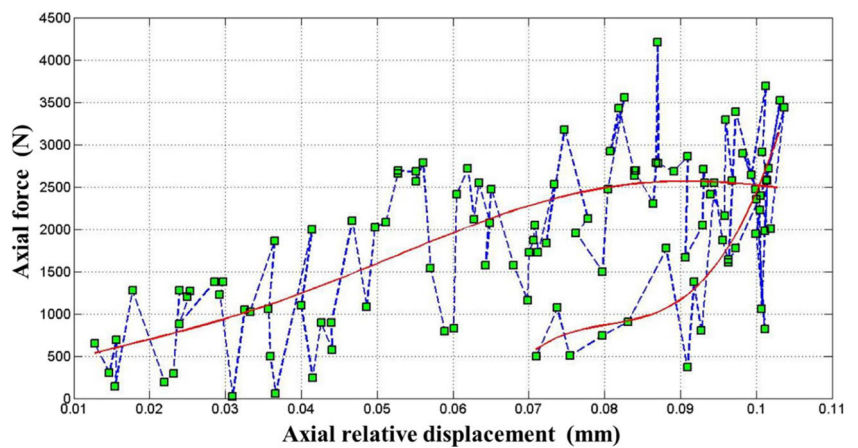
Fig. 12 Axial load-axial relative displacement diagrams of compression members



(a) Compression member ①



(b) Compression member ②

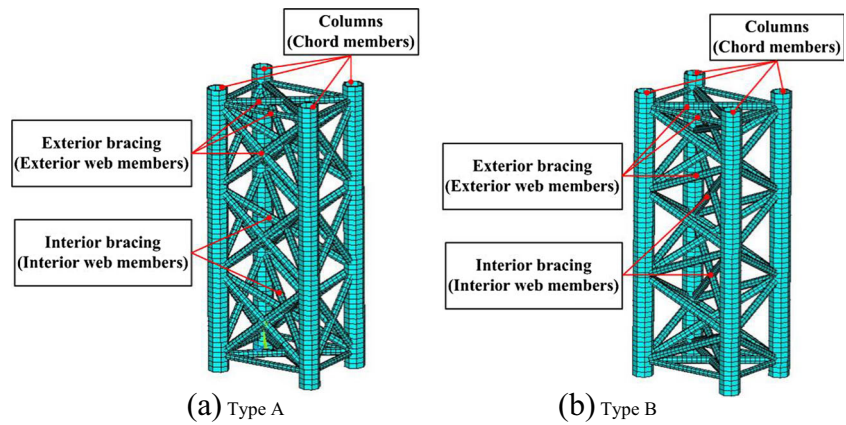


(c) Compression member ③

Figure 12 shows the axial load-axial relative displacement relations of three compression members (denoted as ①, ② and ③ in Fig. 9), and the red lines are polynomial fitting results based on the real testing data (square green points). According to the fitted curve in Fig. 12a, at loading time 102 s, member ① (the lower diagonal web member) gets buckling with the axial force

being -292 N and the axial relative displacement being -0.131 mm. At loading time 180 s, member ② (the lower chord member) becomes unstable, meanwhile its axial force and axial relative displacement are -3285 N and -0.392 mm, respectively (Fig. 12b). Figure 11 denotes that the frame gets global buckling when the vertical displacement of the load-end reaches 1.752

Fig. 13 Initial structures of standard sections



mm, namely at loading time 175 s. Considering the errors introduced in the data collecting and curve fitting process, it is suggested that global buckling and member ② buckling happen simultaneously. In Fig. 12c, at loading time 181 s, member ③ (the upper chord member) begins to be of springback while member buckling does not happen. Therefore, the experimental results of member buckling are consistent with the numerical analysis results, thereby the correctness of the axial stiffness is certified.

Numerical and experimental analysis results demonstrate that the overall stiffness and the axial stiffness can be directly used to quantify structural stability and determine global buckling and compression member buckling effectively. This frame example also indicates that the axial stiffness is capable of detecting the limit point, elastic or elastoplastic, flexural or flexural-torsional buckling of compression members considering only the end forces. Furthermore, the predefined GSI is equivalent to the overall stiffness in quantifying the stability of a static structure during optimization process, because the overall stiffness of initial structure is a constant in Equation (1). Similarly, the proposed MSI is equivalent to the axial stiffness in quantifying the stability of a compression member during optimization process based on Equation (6). Consequently, the proposed stability indices are adequate to evaluate the structural stability quantitatively and

the MSI is applicable to determine the limit point, elastic or elastoplastic, flexural or flexural-torsional buckling of compression members considering only the end forces.

2.4 Anti-buckling mechanism

The boom structure is a special large scale three-dimensional frame. The design strength obtained for each column in a story of a frame should be viewed only as a contribution to the total sway buckling strength of the story, and the structure will sway buckle when the total load on the story exceeds the sum of the individual column contributions (Yura 2006). The actual load distribution on each column does not significantly affect the elastic buckling load, which is the so-called ΣP concept (Yura 2006). Hence, the global buckling will not happen as long as we ensure that all the columns of the frame are in the stable state.

Bracing systems can effectively resist buckling of columns, beams and frames, and the design recommendations cover four general types of bracing systems: relative, discrete, continuous, and lean-on (Galambos 1998). The relative bracing system ((AISC) 2010) is the most common bracing system applied in large scale three-dimensional frame structures, especially in boom structures. Figure 13 shows the initial structures of two typical

Fig. 14 Exterior relative members of a chord member

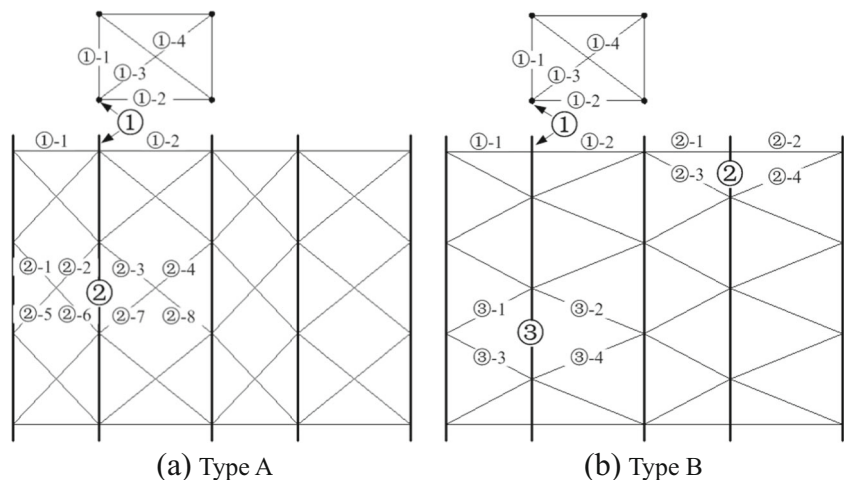
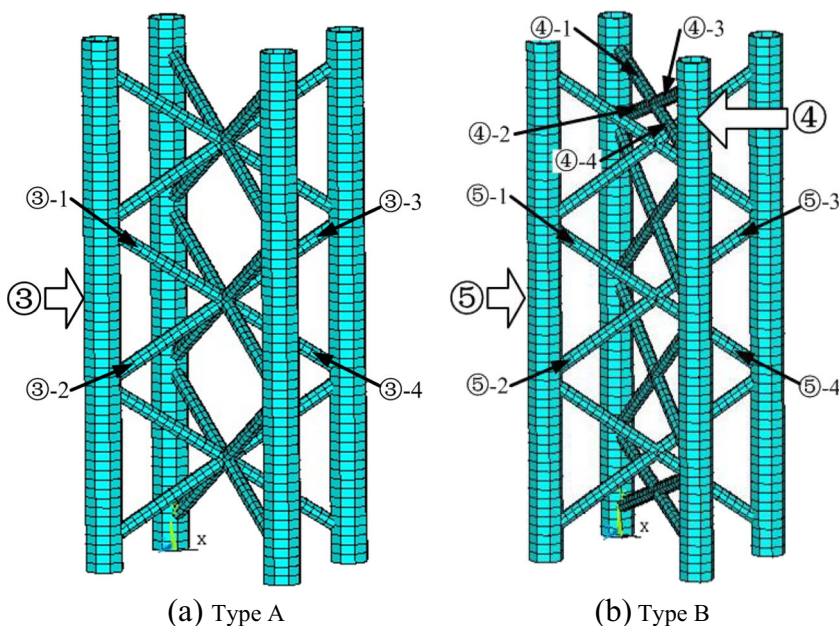


Fig. 15 Interior relative members of a chord member



standard sections of boom structures, which are composed of chord members and web members, and web members can be divided into two parts: exterior web members and interior web members. The exterior web members are located at the six outer surfaces of a standard section, and the other web members are interior web members. The main effect of web members is to enhance the stability of their relative chord members. In order to reinforce the buckling chord members identified through MSI, we present a technique of “freeze”, which means that Young’s modulus is set to the true value of the real material and cannot be modified. Considering the convenience of manufacturing, the exterior web members are easier to be welded on chord members than the interior web members. In the process of topology optimization, when a chord member is judged to be buckling we will first freeze itself and its exterior relative members (Fig. 14), then in the following iteration if the chord member is judged to be buckling again we will freeze its interior relative members (Fig. 15).

3 Optimization procedure

The topology optimization problem of geometrically nonlinear boom structures is expressed mathematically in this section. The formulation of the optimization problem is first presented where the objective function is defined as the discrepancy between the actual structural volume and predetermined target volume. Subsequently, the existing SKO method for bars structures is briefly introduced. Next, the proposed SSKO algorithm is presented in detail for each of the three stages.

3.1 Formulation of the optimization problem

The stability-ensured topology optimization of boom structures with volume and stress considerations can be formulated as follows:

$$\begin{aligned}
 &\text{find} && \mathbf{E} = (E_1, E_2, \dots, E_n)^T \\
 &\text{min} && \left| \sum_{j=1}^n (v_{oj}E_j/E_{\max}) - V_o \times v_{f_{\text{target}}} \right| \quad (j = 1, 2, \dots, n) \\
 &\text{s. t.} && GSI > 0 \\
 &&& MSI_{(j)} > 0 \quad (j = 1, 2, \dots, n) \\
 &&& \sigma_{\max} \leq [\sigma] \\
 &&& E_{\min} \leq E_j \leq E_{\max} \quad (j = 1, 2, \dots, n)
 \end{aligned} \tag{7}$$

Where E_j is the Young’s modulus of member j ($j=1, 2, \dots, n$), v_{oj} is the initial volume of member j , $\sum_{j=1}^n (v_{oj}E_j/E_{\max})$ denotes the total volume of design domain, V_o is the total volume of initial structure in a design domain and $v_{f_{\text{target}}}$ is the

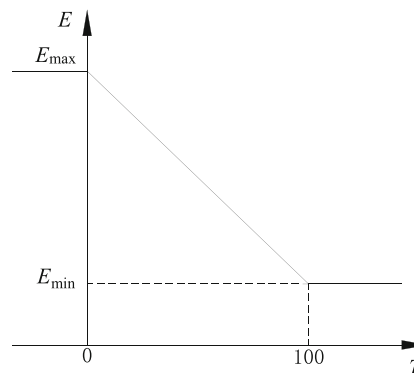
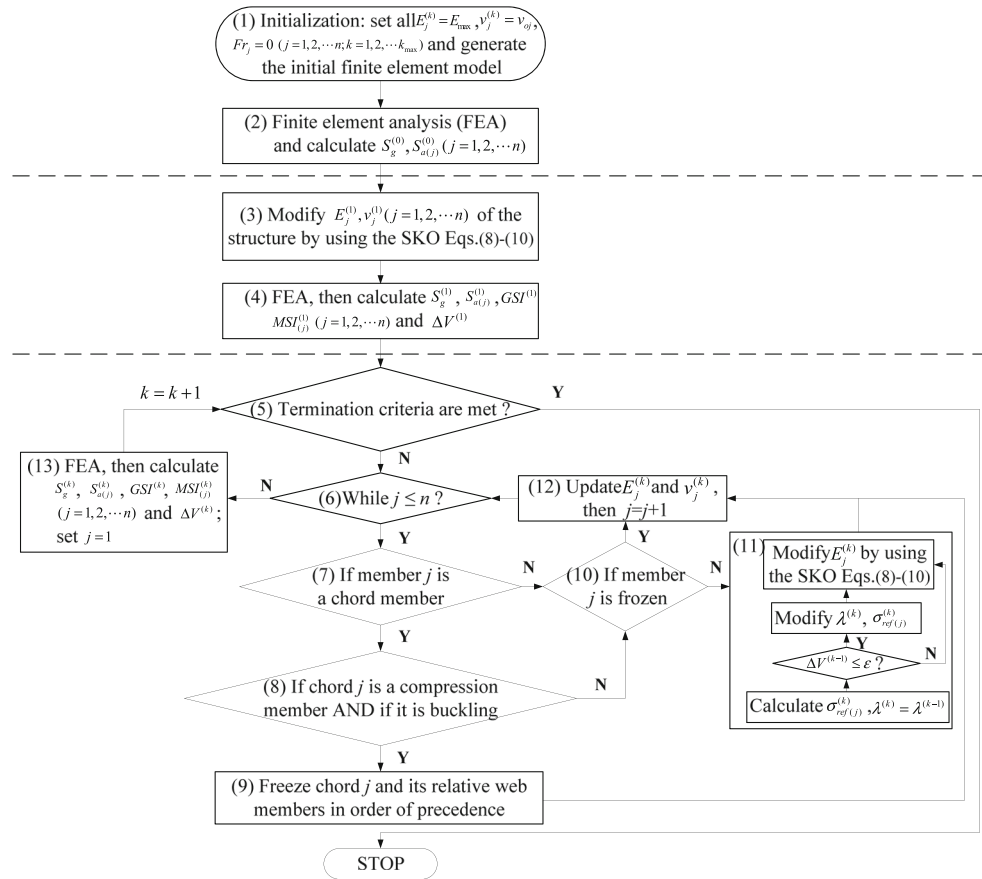


Fig. 16 The E - T relationship

Fig. 17 Flow chart of the SSKO algorithm



predetermined target volume fraction. GSI is the global stability index defined in Equation (1), $MSI_{(j)}$ is member stability index of member j , σ_{max} is the maximum stress, and $[\sigma]$ is the allowable stress. E_{min} and E_{max} are the lower and upper bounds of Young’s modulus, respectively.

3.2 SKO method for bars structures

The SKO method has been used to obtain the optimized design of linear bars structures (Li et al. 2013). Using this method, once the maximum stress and reference stress of bars are obtained after finite element analysis, the temperature index of each bar is calculated by Equations (8)-(10) (Baumgartner et al. 1992; Li et al. 2013). The temperature index has no definite physical meaning, which is an intermediate variable bridging the stress to the Young’s modulus.

$$T_j^{(k)} = \tilde{T}_j^{(k-1)} - s_j^{(k)} \left(\sigma_j^{(k-1)} - \sigma_{ref(j)}^{(k)} \right) \tag{8}$$

$$\tilde{T}_j^{(k-1)} = \begin{cases} 100 & \tilde{T}_j^{(k-1)} \geq 100 \\ 0 & \tilde{T}_j^{(k-1)} \leq 0 \\ \tilde{T}_j^{(k-1)} & \text{otherwise} \end{cases} \tag{9}$$

$$s_j^{(k)} = T_0 / \sigma_{ref(j)}^{(k)} \tag{10}$$

where $\sigma_j^{(k-1)}$ is the maximum stress of member j in the $(k-1)$ -th iteration, and $\sigma_{ref(j)}^{(k)}$ is the reference stress of member j in the k -th iteration. The reference stress equals either the average stress of all bars or the average stress of member j and its adjacent bars in a design domain. In general, the optimization process converges faster by using the latter one as the reference stress, which is thus applied in this paper. $s_j^{(k)}$ is the step factor of member j in the k -th iteration. $T_j^{(k)}$ denotes the temperature index of member j in the k -th iteration, which has a linear relationship with the Young’s modulus (Fig. 16). $T_j^{(0)} = 0$ and $T_0 = 100$.

According to Equations (8)-(10) and Fig. 16, if $\sigma_j^{(k-1)}$ is higher than $\sigma_{ref(j)}^{(k)}$, the temperature index of member j will be reduced and its Young’s modulus will be increased; otherwise, the Young’s modulus of member j will be reduced. When $T_j^{(k-1)} \leq 0$, $E = E_{max}$ is the real material Young’s modulus. When $T_j^{(k-1)} \geq 100$, $E = E_{min} = E_{max}/1000$ (Baumgartner et al. 1992). The SKO method has a natural penalization feature due to the polarization of reference stresses of members during an optimization process. Based on Equations (8)-(10) and Fig. 16, the stress of a member will approach its reference stress. As a result, the temperature indices and the Young’s modulus of members also exhibit polarization during the optimization process. Besides, the termination criteria require that the Young’s modulus of each member converges to an

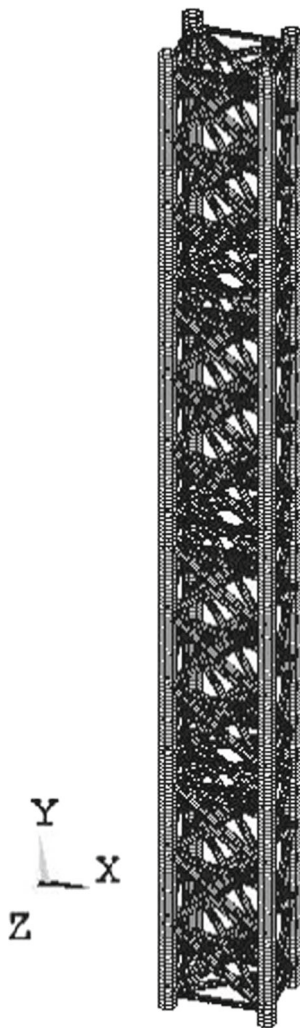


Fig. 18 A four-section frame

invariant (Equation (11)). Thus, the convergent result has no bars with an intermediate Young's modulus. Lots of benchmark examples and industrial applications solved by the SKO method have demonstrated this point (Baumgartner et al. 1992; Harzheim and Graf 2005, 2006; Li et al. 2013).

3.3 Stability-ensured soft kill option (SSKO) algorithm

In order to realize topology optimization and guarantee global stability of boom structures, this paper proposes a novel SSKO algorithm based on the SKO method for bars structures, stability indices and anti-buckling mechanism. The SSKO algorithm is a fully stressed topology optimization method with volume and stress considerations. The method is divided into three stages: initial analysis, preliminary optimization, and stability-ensured optimization, shown in Fig. 17. Superior to other algorithms, SSKO detects the buckling chord members through MSI and subsequently freezes them and their relative web members during the stability-ensured optimization stage. A growth factor of the reference

stress is introduced as a step function with respect to the iteration number to adjust the speed of optimization. All details will be explained in the following.

In the initial analysis stage (STEPS 1–2), this algorithm defines an initial finite element model and conducts geometrically nonlinear analysis, then calculates the overall stiffness $S_g^{(0)}$ and the axial stiffness of each compression member (Equation (5)). $Fr_j=0$ means that member j is not frozen, and $Fr_j=1$ means member j is frozen. In the preliminary optimization stage (STEPS 3–4), the Young's modulus of each member is modified by the SKO Equations (8)–(10) directly, then the finite element analysis of the structure is carried out. Afterwards, the overall stiffness, the axial stiffness of compression members, GSI, MSI and the total volume change are calculated as the references of the subsequent optimization iterations. The stability-ensured optimization stage is the key part of SSKO algorithm, and the detailed procedure from STEP 5 to STEP 13 is provided in the following.

STEP 5: If any of the following criteria (Equations (11)–(14)) is met, stop the procedure. Otherwise, move to STEP 6.

$$\begin{aligned} \Delta V^{(k-1)} &= |V^{(k-1)} - V^{(k-2)}| \leq \varepsilon \text{ and } \Delta V^{(k-2)} \\ &= |V^{(k-2)} - V^{(k-3)}| \leq \varepsilon \end{aligned} \quad (11)$$

$$vf^{(k-1)} \leq vf_{\text{target}} \text{ and } \Delta V^{(k-1)} \leq \varepsilon \quad (12)$$

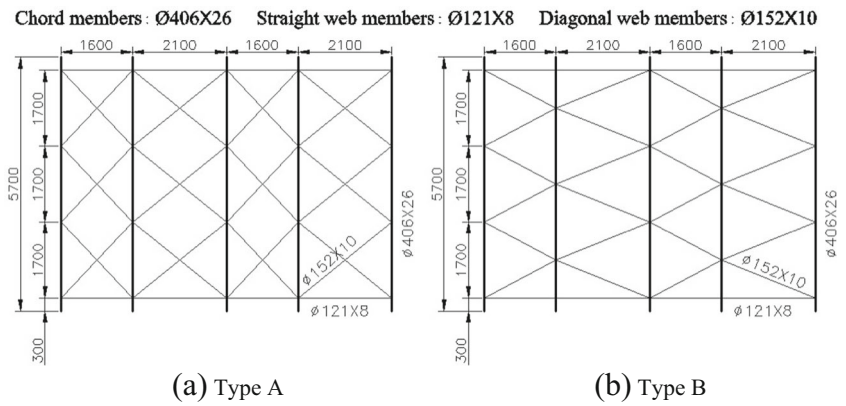
$$\sigma_{\text{max}}^{(k-1)} \geq [\sigma] \quad (13)$$

$$k > k_{\text{max}} \quad (14)$$

In Equation (11), the tolerance of total volume change ε is a sufficiently small positive real number. The total volume change among the last three iterations should be lower than ε . The volume fraction in the last iteration reaches the target volume fraction and the total volume change in the last iteration is lower than the tolerance, as shown in Equation (12). Generally, the total volume change is required to be equal to zero in order to get a topology with the steady distribution of Young's modulus. The maximum stress in the last iteration is greater than the allowable stress (Equation (13)). The maximum iteration number k_{max} is a sufficiently large positive integer. If the iteration number k becomes larger than k_{max} , the procedure terminates.

STEP 6–STEP12: Check all members in a design domain one by one, and update the Young's modulus of each member. STEP 8 is to judge whether chord j is buckling by Equation (6), and STEP 9 is to freeze chord j and its relative web members according to the anti-buckling mechanism discussed in Section 2. If member j is not frozen, the procedure goes to STEP 11 and the Young's modulus of member j can be modified by the SKO Equations (8)–(10). The reference stress $\sigma_{ref(j)}^{(k)}$ in the SKO equations should be raised by Equations (15)–(17) to make the structure to be close to the target volume

Fig. 19 Dimensions of standard sections



fraction if the total volume change in the last iteration is lower than ε .

$$\sigma_{ref(j)}^{(k)} = \sigma_{ref(j)}^{(k-1)} \lambda^{(k)} \tag{15}$$

$$\lambda^{(k)} = \lambda^{(k-1)} + \Delta\lambda^{(k)} \tag{16}$$

$$\Delta\lambda^{(k)} = \frac{1 - v_f^{(k-1)}}{1 - v_f^{target}} \Delta\lambda_{max} \tag{17}$$

Here, $\lambda^{(k)}$ denotes the growth factor of the reference stress, and $\lambda^{(0)} = 1$. $\Delta\lambda^{(k)}$ means the increment of the growth factor, and $\Delta\lambda_{max}$ is the maximum increment of the growth factor in each iteration, such as $\Delta\lambda_{max} = 0.15$. When the volume fraction of the structure becomes closer to the target volume fraction, the increment of the growth factor gets larger.

The modified reference stress may be larger than the allowable stress sometimes, so this procedure records the original reference stress $\sigma_{ref}^{(k)} = \sigma_{ref(j)}^{(k)} \lambda^{(k)}$, then adjusts the reference stress and the growth factor by Equations (18)-(19).

$$\sigma_{ref(j)}^{(k)} = [\sigma] \tag{18}$$

$$\lambda^{(k)} = [\sigma] / \sigma_{ref}^{origin} \tag{19}$$

At last, $E_j^{(k)}$ is updated in STEP 12. If member j is frozen, $E_j^{(k)}$ will be set to the Young's modulus of the real material; otherwise, $E_j^{(k)}$ will be set to the computing result from STEP 11. Meanwhile, $v_j^{(k)}$ is updated by $v_j^{(k)} = v_{oj} E_j^{(k)} / E_{max}$.

STEP 13: Execute FEA, then calculate $S_g^{(k)}$, $S_{a(j)}^{(k)}$, $GSI^{(k)}$, $MSI_{(j)}^{(k)} (j = 1, 2, \dots, n)$ and $\Delta V^{(k)}$. Reset $j = 1$, go back to STEP 5.

4 Illustrative examples

4.1 Four-section frames

We studied two four-section frames to compare optimization effectiveness of the existing SKO method and the proposed SSKO algorithm. One four-section frame is composed of type A standard sections (Fig. 13a), and the other is composed of type B standard sections (Fig. 13b). As shown in Fig. 18, a four-section frame is a column structure stacked by four standard sections which is modeled in the FE package ANSYS 13.0. All bars are rigidly connected at nodes and the beam189 element, a 3-D quadratic three-node beam element, is selected to simulate the bars. The dimensions are shown in Fig. 19, and the Young's modulus is 206GPa. The four bottom points of

Table 1 The performances of SKO method and SSKO algorithm in four-section problems

Methods	Scenario	v_f^{target}	$\Delta\lambda_{max}$	$[\sigma]$	GSI	Volume fraction	Max. stress	Number of iterations
SKO	A-1	—	—	—	buckling	0.6692	350.47	4
	B-1	—	—	—	buckling	0.6396	475.93	2
SSKO	A-2	0.80	0.15	500	0.9728	0.7913	385.20	32
	A-3	0.60	0.15	500	0.9728	0.7913	385.20	35
	A-4	0.60	0.60	500	0.9728	0.7913	385.20	27
	A-5	0.60	1.00	500	0.9728	0.7913	385.20	24
	B-2	0.80	0.15	600	0.9798	0.8426	304.02	12
	B-3	0.60	0.15	600	0.9798	0.8426	304.02	12
	B-4	0.60	0.30	600	0.9798	0.8426	304.02	12
	B-5	0.60	0.90	600	0.9798	0.8426	304.02	12

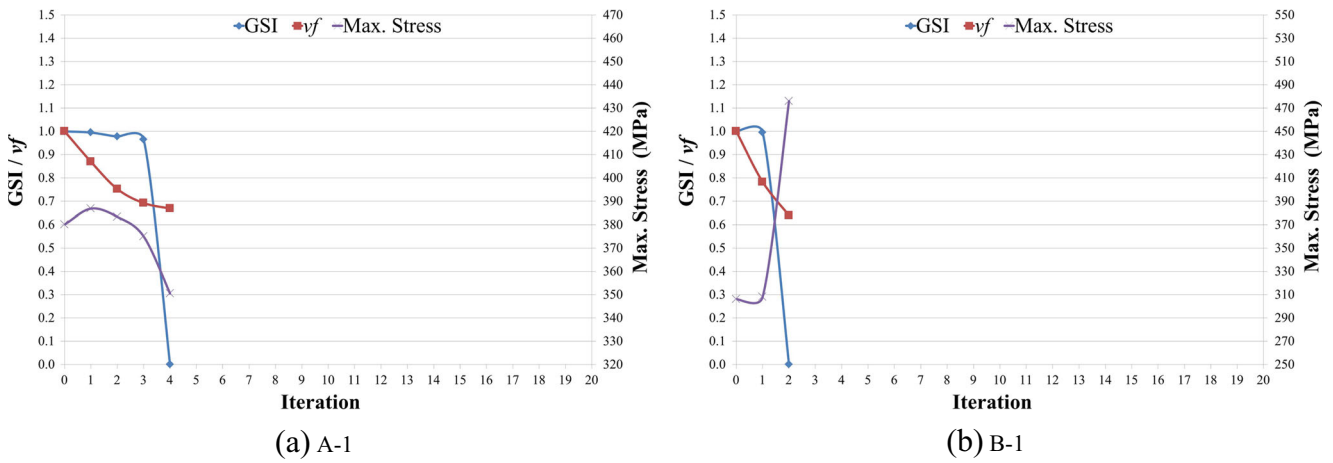


Fig. 20 Optimization history of the SKO method in four-section frame problems

frame are fixed, a vertical force of 8000KN is applied downward (-Y) at each top point, and a horizontal force of 10KN is

applied rightward (+X) at each end point of left-side chord members. The gravitational load is also included in this study.

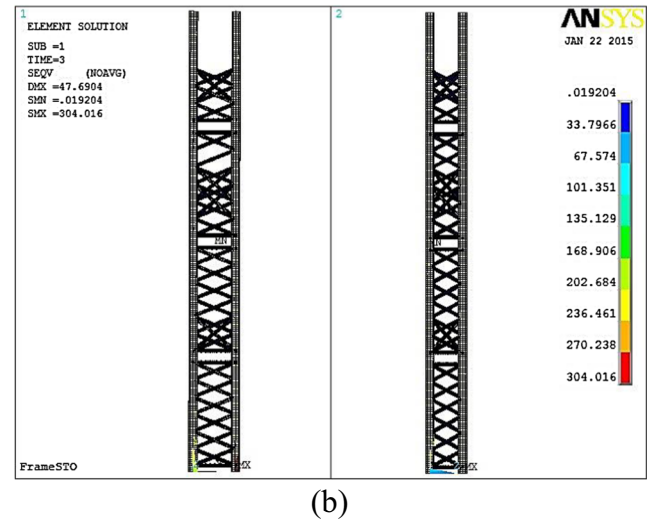
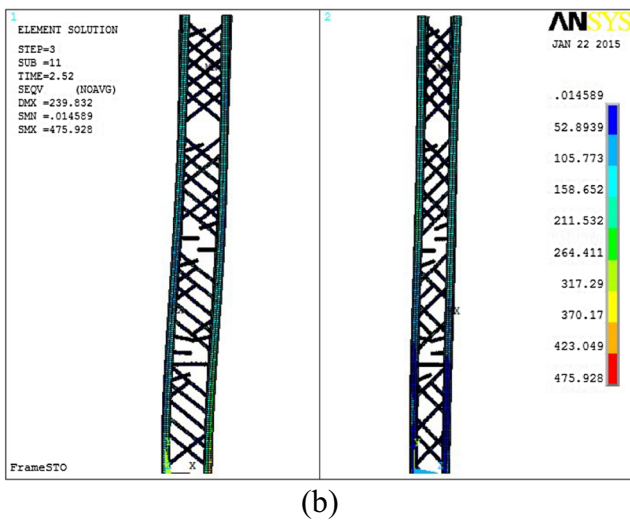
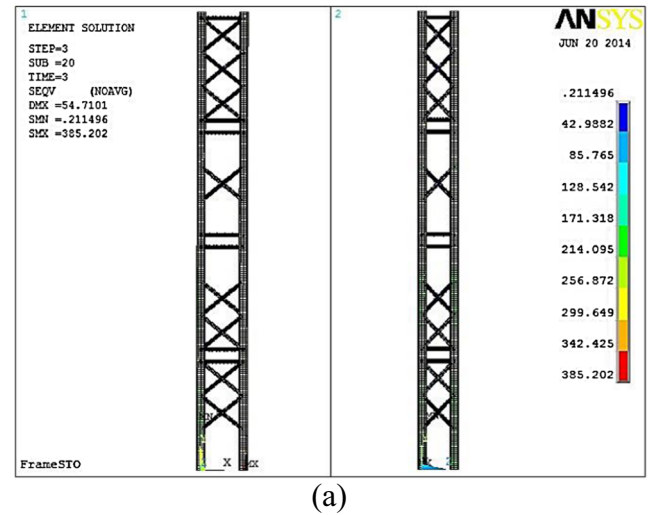
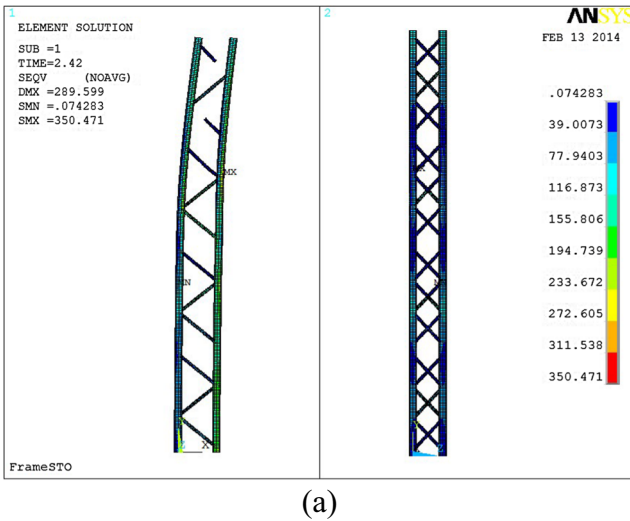


Fig. 21 Optimization results of four-section frames by using the SKO method a Type A b Type B

Fig. 22 Optimization results of four-section frames by using the SSKO method a Type A b Type B

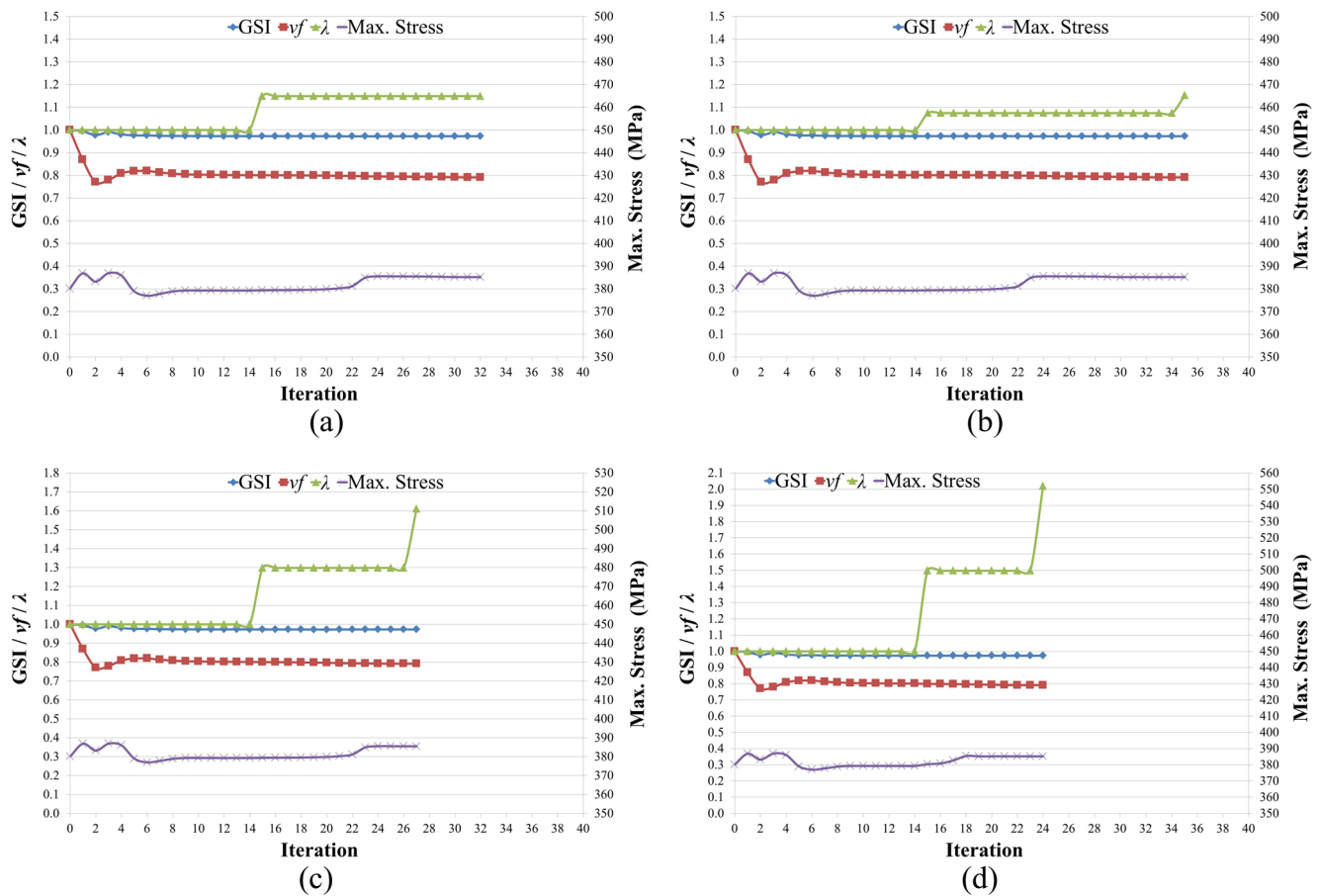


Fig. 23 Convergence histories of SSKO algorithm in type A frame problem by scenarios **a** A-2 **b** A-3 **c** A-4 **d** A-5, respectively

The mechanical model of the four-section frame is a geometrically-nonlinear elastic static model, and the structures are analyzed by the incremental load method and the Newton–Raphson method.

The results obtained by the SKO method and the SSKO algorithm are listed in Table 1. Several scenarios with different target volume fractions and maximum increments of the growth factor are employed in these benchmark examples. The optimization histories and topologies of SKO method are depicted in Figs. 20 and 21. The topologies and convergence histories of SSKO algorithm by four scenarios are shown in Figs. 22, 23 and 24. It should be noticed that in convergent topologies all the reserved bars have the maximum Young’s modulus and all the removed bars have the minimum Young’s modulus (Fig. 22), but there are some bars with intermediate Young’s modulus in the unsuccessful optimization results while their removed bars have the minimum Young’s modulus (Fig. 21).

The optimization process fails at the beginning due to global buckling when the SKO method is applied. Figure 21 are stress distribution of the buckling models, which contain two parts: the left half part is the XY plane view, and the right half part is the YZ plane view. It shows that a lot of members are removed from the four-section

frames as a result of not considering stability. The volume fractions reduce significantly while GSIs decrease sharply (see Fig. 20).

Figure 22 shows the stress distribution of the topologies obtained by SSKO algorithm. Whatever scenario is adopted in SSKO algorithm, the optimization result of each type of frame is the same, which shows that the proposed SSKO algorithm is steady and reliable. However, the convergence histories of the SSKO algorithm by different scenarios are not consistent with each other (see Figs. 23 and 24).

The SSKO algorithm guarantees the global stability of the frame in the optimization process which is reflected through the GSI curve shown in Figs. 23 and 24. For the type A frame, the target volume fraction vf_{target} is set to 0.8 in scenario A-2, and the volume fraction becomes lower than 0.8 in the 2nd and the 3rd iterations and after the 18th iteration, but the optimization procedure does not stop because there is still a remarkable total volume change in these iterations (Equation (12)). Similar situations occur in optimization processes by using scenario B-2. The growth factor of the reference stress λ is a step function of iteration number, and the maximum increment of the growth factor $\Delta\lambda_{max}$ is set to be different values within scenarios A-3, A-4 and A-5. The larger the maximum increment of the growth factor is, the faster the

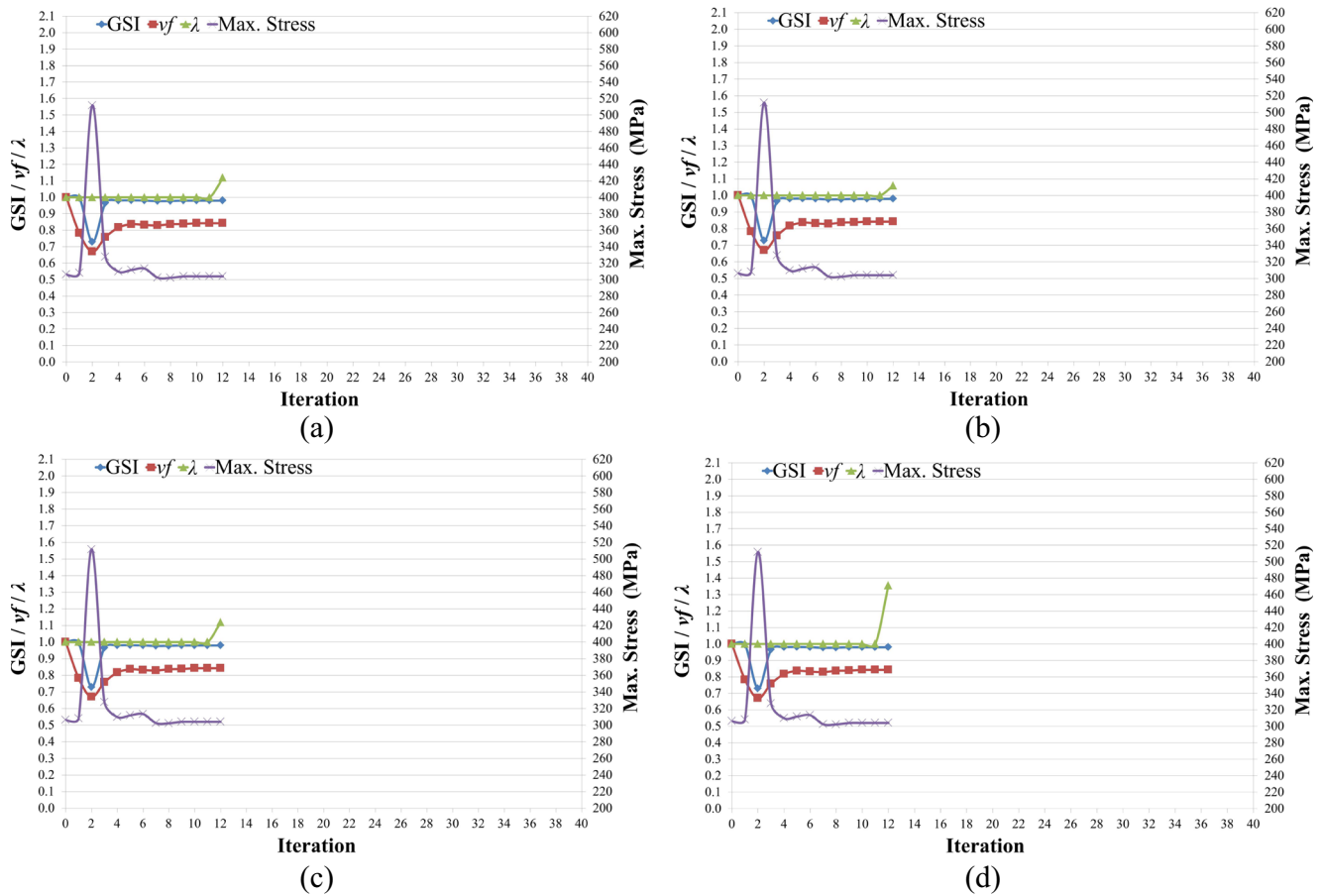


Fig. 24 Convergence histories of SSKO algorithm in type B frame problem by scenarios **a** B-2 **b** B-3 **c** B-4 **d** B-5, respectively

convergence is. Nonetheless, the optimization process converges at the same iteration as for the type B frame because this type of frame has less web members and they are freed quickly when buckling chord members are detected. Besides, $\Delta\lambda_{\max}$ cannot be unrestrictedly large which will cause severe

instability of optimization. This will be discussed later in Section 4.2 with the boom structure problem. The allowable stress is selected appropriately to be greater than the maximum stress of the initial structure, and the variation of the maximum stress is not large from the 3rd iteration (see Figs. 23 and 24),

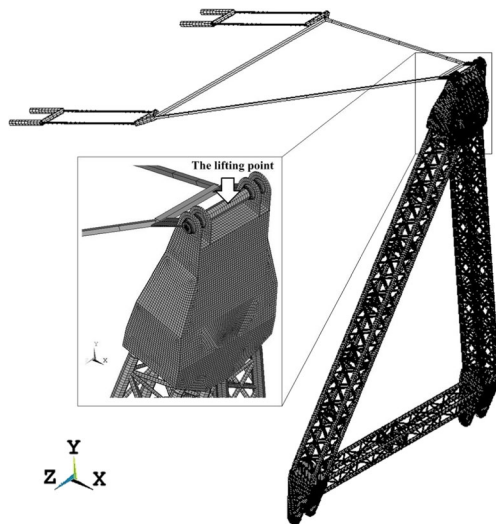


Fig. 25 45.5m boom structure

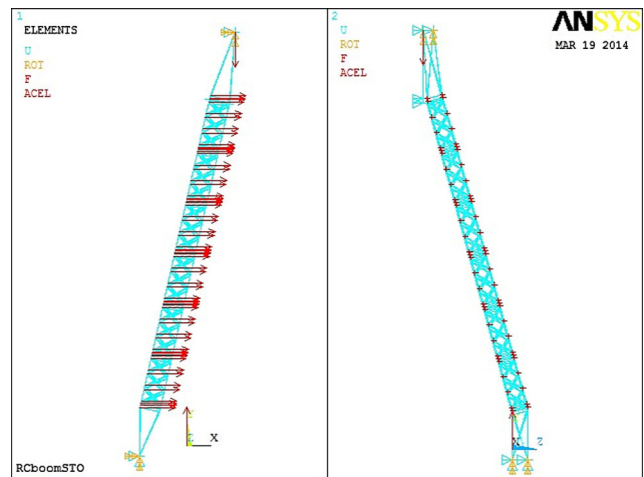


Fig. 26 Finite element model of 45.5m half-boom

Table 2 The performances of SSKO algorithm in boom structure problem

Methods	Scenario	v_{target}	$\Delta\lambda_{max}$	$[\sigma]$	GSI	Volume fraction	Max. stress	Number of iterations
SSKO	C-1	0.5	0.90	500	0.8969	0.8163	571.14	141
	C-2	0.5	0.30	500	0.9860	0.7823	173.68	84
	C-3	0.5	0.15	500	0.9860	0.7823	173.68	129

so the stress constraint can be always satisfied in this case studies.

4.2 Boom structure

A 45.5m-long combined boom of 2500-tonne ring crane (see Fig. 25) is studied as an example of complex structure system. All the twelve standard sections are replaced by type A standard sections (Figs. 13a and 19a). Considering the symmetry of the combined boom, only half structure is analyzed.

Figure 26 shows the finite element model of the half-boom in ANSYS 13.0. The left part of Fig. 26 is the view of the luffing plane (XY plane), and the right part is the view of the swing plane (YZ plane). The bars of the combined boom are steel circular pipes and they are rigidly connected at nodes. The beam189 element, a 3-D quadratic three-node beam element based on Timoshenko beam theory, is selected to simulate the bars of the combined boom. The range of the boom is 10m (“range” refers to the horizontal distance between the center of boom foot pins and boom tip pins), a lifting load $F_Q=14320000N$ is applied at the lifting point, and a +X direction wind load $F_W=26778N$ is uniformly distributed on end points of chord members of standard sections. The mechanical model of the boom is geometrically nonlinear elastic static model, and the structure is analyzed by the incremental load method and the Newton–Raphson method.

In order to improve the calculation efficiency, the plate structures at the ends of the boom are simplified as rigid bars, which belong to non-design domain. At the top of boom, only the Z-axis rotational and Y-axis translational degrees of freedom are released. At the bottom of boom, only the Z-axis rotational degree of freedom is released. At the symmetry plane of the whole combined boom, the Z-axis translational degree of freedom is constrained.

Three scenarios are applied in the topology optimization of this boom structure, and their performances are listed in Table 2. Based on the experience from the previous case study, we make $\Delta\lambda_{max}$ equal a large number in scenario C-1, intentionally to get a fast convergence speed, but it turns out not to be the case. Figure 27 is the optimization results using scenario C-1 (The layout of Figs 27 and 29 is the same as Fig. 26). It is obvious that this topology is not the optimal solution because the stress of most retained members is lower than 380MPa and the maximum stress which is above 500MPa happens at a local connection area (see Fig. 27a). Figure 28 shows that the maximum stress begins to fluctuate divergently from the 40th iteration and goes beyond the allowable stress in 141st iteration resulting in termination of optimization process. The GSI decreases to a minimum of 0.5465 in 139th iteration but the structure still keeps stable. The volume fraction also begins to fluctuate divergently from the 40th iteration as a result of the growth factor of the reference stress λ exceeding 2.5. When the growth factor becomes large, the reference stress gets an enormous growth at each step that leads to a sharp decrease of the volume fraction (Equation (8)). It

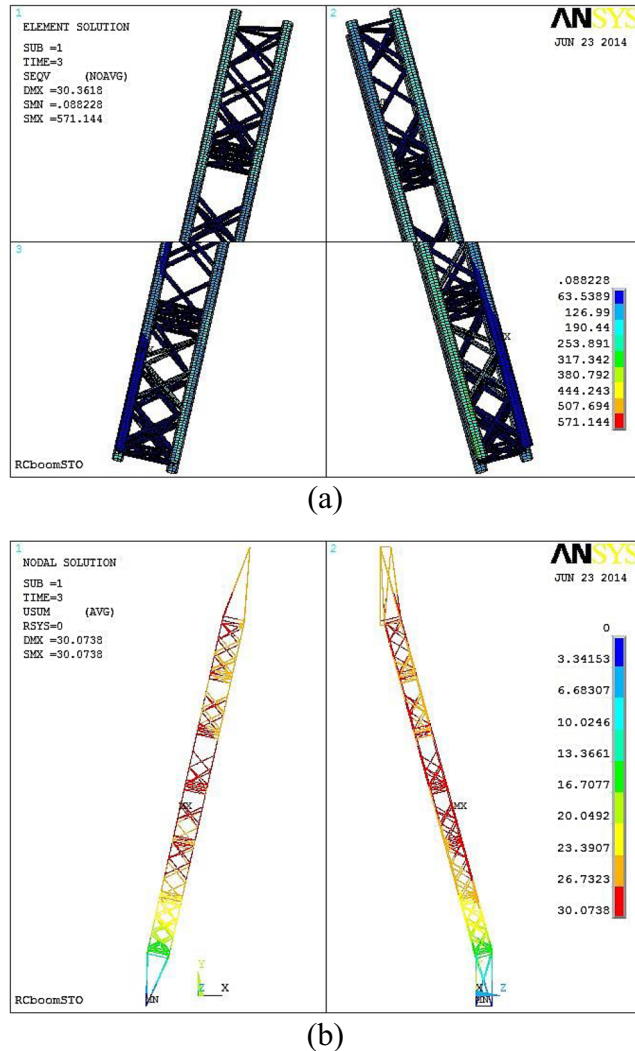
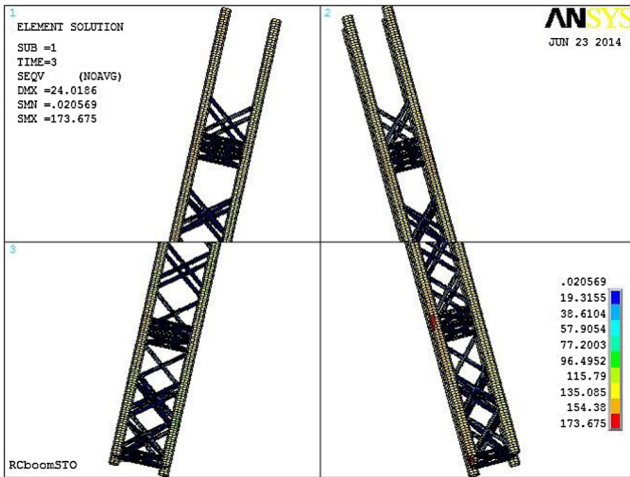
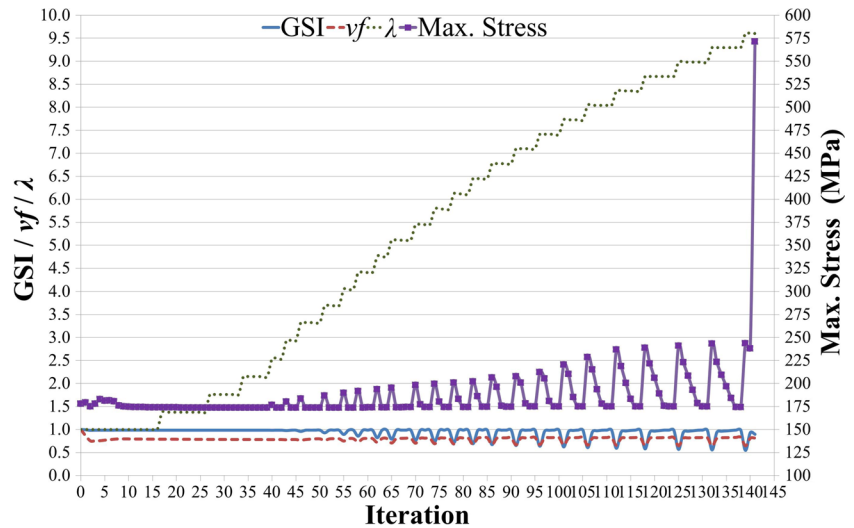
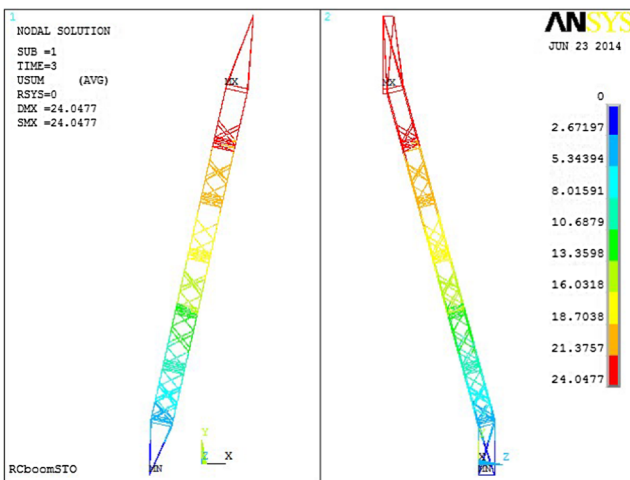


Fig. 27 Optimization results of boom structure by scenario C-1 **a** von Mises stress **b** displacement

Fig. 28 Optimization history of SSKO algorithm in boom structure problem by scenario C-1



(a)



(b)

Fig. 29 Optimization results of boom structure by either scenario C-2 or C-3 **a** von Mises stress **b** displacement

means that a considerable portion of material is softened which usually causes the occurrence of stress concentration (see Fig. 27a). The maximum stresses of many members become higher than the reference stress in the subsequent iterations, so the volume fraction increases after its significant decrease. It has also been demonstrated by other case studies we conducted that under most circumstances λ should not be larger than 2.5 in order to ensure the stability of optimization.

The maximum increment of the growth factor is reduced in scenarios C-2 and C-3 to make the optimization process more stable. The optimization results (see Fig. 29) are the same by either scenario C-2 or C-3, which justifies the proposed SSKO algorithm. Figure 30 shows the convergence histories of the SSKO algorithm in boom structure problem by strategies C-2 and C-3 respectively. The procedures converge after several step growths of λ , and the scenario C-2 has a higher optimization efficiency than the scenario C-3. The anti-buckling mechanism works well since the GSI keeps at around 1. The volume fraction decreases to 0.7823 and the maximum stress becomes 173.68MPa eventually. Same as the example of four-section frames in Section 4.1, we should notice that in convergent topologies all reserved bars have the maximum Young's modulus and all removed bars have the minimum Young's modulus (Fig. 29), but there are some bars with intermediate Young's modulus in the unsuccessful optimization results while their removed bars have the minimum Young's modulus (Fig. 27).

The SSKO algorithm works well in topology optimization of boom structures as long as we select an appropriate maximum increment of the growth factor. The algorithm reduces the total volume significantly and gives a stable optimized design with the maximum stress being lower than the predetermined stress limit. These examples also demonstrate applicability and practical efficiency of the SSKO algorithm since it converges to the same result through only a few dozens of iterations.

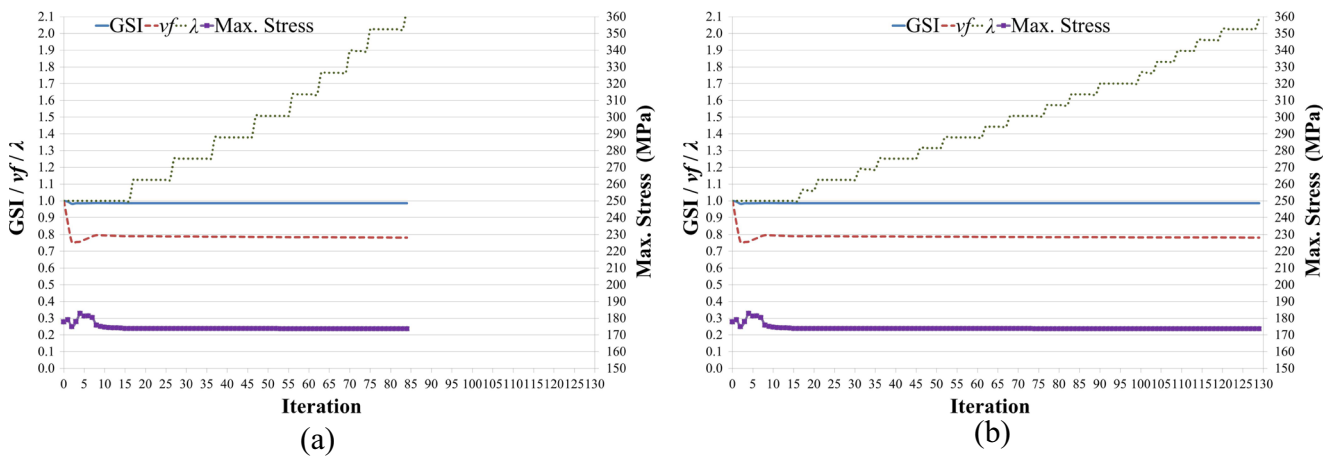


Fig. 30 Convergence histories of SSKO algorithm in boom structure problem by scenarios **a** C-2 **b** C-3, respectively

5 Conclusions

This paper presents a Stability-Ensured Soft Kill Option (SSKO) algorithm for structural topology design of geometrically nonlinear boom structures including volume and stress considerations. This algorithm is developed for large-scale boom structures by employing the proposed compression member stability index (MSI) and the knowledge of bracing systems for resisting buckling of columns. The MSI can be used to distinguish limit-point buckling of various kinds of compression members and has been applied for judging the buckling of compression chord members in this work. The global stability is guaranteed through orderly freezing the relative web members of any buckling chord member found, and the proper freezing order of relative web members should be developed according to the specific initial structure. Besides, the global stability index (GSI) is defined to evaluate global stability status of the whole structure quantitatively and we conducted numerical and experimental verifications of two stability indices through nonlinear buckling analysis of a simple frame.

The SSKO algorithm contains a growth factor of the reference stress which is a step function of the iteration number. Its sole purpose is to further remove materials from the optimized structure. The volume fraction is optimized to be as close as possible to the predefined target volume fraction subject to stability and stress constraints. Incorporating both stability and stress constraints is important to ensure the feasibility of final topology designs.

Two examples are studied by using different scenarios to investigate performances of the proposed SSKO algorithm. The results of the four-section frame problems exhibit its stability-ensured effect and practically acceptable convergence speed. The boom structure problem indicates that an appropriate maximum increment of the growth factor plays a crucial role in converging to the optimized design. The consistent optimization results in different scenarios demonstrate

the potential of the SSKO algorithm to be generally applicable.

This paper extends the fully stressed SKO method to the stability-ensured SKO algorithm by integrating GSI and MSI which are verified by numerical analysis and physical experiment. It is demonstrated that they are capable of detecting buckling of various kinds of nonlinear static bars structures. In addition, despite that our research focuses on multi-section frames and boom structures, the SSKO algorithm can be easily modified for topology optimization of other types of large-scale bars structures, such as truss tower, reticulated structure, truss bridge, etc. Specifically, the anti-buckling mechanism (freezing relative web members for boom structures) can be modified to fit the specific class of structure, meanwhile the buckling can still be identified by tracing changes of GSI and MSI. Furthermore, the SSKO approach is easy to implement in commercial software, thus it is suitable for topology optimization of complex large-scale engineering applications. Consequently, the proposed SSKO algorithm has a great potential of becoming a general stability-ensured topology optimization method for large-scale bars structures.

Acknowledgments Funding for this research was provided by the National Natural Science Foundation of China (NSFC) under award number 51375345. Financial support for the first author, Wenjun Li, was provided in part by the China Scholarship Council. The views expressed are those of the authors and do not necessarily reflect the views of the sponsors.

References

- American Institute of Steel Construction (AISC) (2010) Specification for structural steel buildings ANSI/AISC 360–10. AISC, Chicago, USA
- Baumgartner A, Harzheim L, Mattheck C (1992) SKO (Soft Kill Option) - the biological way to find an optimum structure topology. *Int J Fatigue* 14(6):387–393

- Bojczuk D, Mroz Z (1999) Optimal topology and configuration design of trusses with stress and buckling constraints. *Struct Optim* 17(1):25–35
- Browne PA, Budd C, Gould NIM, Kim HA, Scott JA (2012) A fast method for binary programming using first-order derivatives, with application to topology optimization with buckling constraints. *Int J Numer Methods Eng* 92(12):1026–1043
- Chen J (2011) Stability of steel structures theory and design. Science Press, Beijing, Fifth Edition edn [In Chinese]
- Cheng G (2012) Introduction to optimum design of engineering structures. Dalian University of Technology Press, Dalian [In Chinese]
- Duysinx P, Sigmund O (1998) New developments in handling stress constraints in optimal material distribution. Paper presented at the 7th AIAA/USAF/NASA/ISSMO Symposium on Multidisciplinary Analysis and Optimization, St. Louis, MO
- Eschenauer HA, Olhoff N (2001) Topology optimization of continuum structures: a review. *Appl Mech Rev* 54(4):331–390
- Fan F, Yan J, Cao Z (2012) Stability of reticulated shells considering member buckling. *J Constr Steel Res* 77:32–42
- Galambos TV (1998) Guide to stability design criteria for metal structures, 5th edn. Wiley, USA
- Harzheim L, Graf G (2005) A review of optimization of cast parts using topology optimization - I - topology optimization without manufacturing constraints. *Struct Multidiscip Optim* 30(6):491–497
- Harzheim L, Graf G (2006) A review of optimization of cast parts using topology optimization - II - topology optimization with manufacturing constraints. *Struct Multidiscip Optim* 31(5):388–399
- Hjelmstad KD, Pezeshk S (1991) Optimal design of frames to resist buckling under multiple load cases. *J Struct Eng ASCE* 117(3):914–935
- Kemmler R, Lipka A, Ramm E (2005) Large deformations and stability in topology optimization. *Struct Multidiscip Optim* 30(6):459–476
- Lawrence KL (2011) ANSYS tutorial release 13. Stephen Schroff, Mission
- Li WJ, Zhou QC, Zhang XH, Xiong XL, Zhao J (2013) Topology optimization design of bars structure based on SKO method. *Applied Mechan Mat* 394(1):515–520
- Li WJ, Zhao J, Jiang Z, Chen W, Zhou QC (2015) A numerical study of the overall stability of flexible giant crane booms. *J Constr Steel Res* 105:12–27
- Lin C-Y, Sheu F-M (2009) Adaptive volume constraint algorithm for stress limit-based topology optimization. *Comput Aided Des* 41(9):685–694
- Lindgaard E, Dahl J (2013) On compliance and buckling objective functions in topology optimization of snap-through problems. *Struct Multidiscip Optim* 47(3):409–421
- Lindgaard E, Lund E (2010) Nonlinear buckling optimization of composite structures. *Comput Methods Appl Mech Eng* 199(37–40):2319–2330
- Lindgaard E, Lund E (2011) A unified approach to nonlinear buckling optimization of composite structures. *Comput Struct* 89(3–4):357–370
- Lund E (2009) Buckling topology optimization of laminated multi-material composite shell structures. *Compos Struct* 91(2):158–167
- Manickarajah D, Xie YM, Steven GP (2000) Optimisation of columns and frames against buckling. *Comput Struct* 75(1):45–54
- Mase GT, Mase GE (1999) Continuum mechanics for engineers, 2nd edn. CRC Press, New York
- Ohsaki M, Ikeda K (2007) Stability and optimization of structures generalized sensitivity analysis. Springer, New York
- Pyrz M (1990) Discrete optimization of geometrically nonlinear truss structure under stability constraints. *Struct Optimiz* 2(2):125–131
- Rozvany GIN, Sobieszcanski-Sobieski J (1992) New optimality criteria methods: forcing uniqueness of the adjoint strains by corner-rounding at constraint intersections. *Struct Optimiz* 4(3):244–246
- Shen Z, Su C, Luo Y (2007) Application of strut model on steel spatial structure. *Building Struct* 37(1):8–11 [In Chinese]
- Sigmund O, Maute K (2013) Topology optimization approaches - a comparative review. *Struct Multidiscip Optim* 48(6):1031–1055
- The electronic universal testing machine RGM-4300. (2014) REGER. <http://www.reger.com.cn>
- The VIC-3D System. (2014) Correlated Solutions, Inc. <http://www.correlatedsolutions.com>
- Tortorelli DA, Michaleris P (1994) Design sensitivity analysis: overview and review. *Inverse Prob Eng* 1(1):71–105
- Yura JA (2006) Five Useful Stability Concepts. Paper presented at the Proceedings of the 2006 Structural Stability Research Council Annual Stability Conference, San Antonio, Texas